Nonlinear dynamics of direction-selective recurrent neural media

Xiaohui Xie[1,*] and Martin A. Giese[1,2]
[1]*Department of Brain and Cognitive Sciences and Center for Biological and Computational Learning, Massachusetts Institute of Technology, Cambridge, Massachusetts 02139*
[2]*Department for Cognitive Neurology, University Clinic Tübingen and Max-Planck Institute for Biological Cybernetics, 72076 Tübingen, Germany*

(Received 11 December 2001; revised manuscript received 5 March 2002; published 3 May 2002)

The direction selectivity of cortical neurons can be accounted for by asymmetric lateral connections. Such lateral connectivity leads to a network dynamics with characteristic properties that can be exploited for distinguishing in neurophysiological experiments this mechanism for direction selectivity from other possible mechanisms. We present a mathematical analysis for a class of direction-selective neural models with asymmetric lateral connections. Contrasting with earlier theoretical studies that have analyzed approximations of the network dynamics by neglecting nonlinearities using methods from linear systems theory, we study the network dynamics with nonlinearity taken into consideration. We show that asymmetrically coupled networks can stabilize stimulus-locked traveling pulse solutions that are appropriate for the modeling of the responses of direction-selective neurons. In addition, our analysis shows that outside a certain regime of stimulus speeds the stability of these solutions breaks down, giving rise to lurching activity waves with specific spatiotemporal periodicity. These solutions, and the bifurcation by which they arise, cannot be easily accounted for by classical models for direction selectivity.

DOI: 10.1103/PhysRevE.65.051904 PACS number(s): 87.19.La, 87.18.Sn, 87.10.+e

I. INTRODUCTION

Most classical models for the direction selectivity of cortical neurons have assumed feedforward mechanisms, such as multiplication or gating of afferent thalamo-cortical inputs (e.g. [1–3]), or linear spatiotemporal filtering followed by a nonlinear operation, such as squaring (e.g. [4,5]). More recently, the existence of strong lateral connectivity has motivated modeling studies that show that the properties of direction selective cortical neurons can also be reproduced by recurrent neural network models with asymmetric lateral excitatory or inhibitory connections [6,7].

The relative contribution of feedforward and recurrent connectivity to the direction selectivity of cortical neurons remains an unresolved issue. In this paper we provide a different perspective by presenting a mathematical analysis of the nonlinear dynamics that arises in simple nonlinear neural networks with asymmetric recurrent connections that are driven by moving input stimuli. We show that such networks have a class of form-stable solutions, in the following signified as *stimulus-locked traveling pulses*. The amplitude of these traveling pulse solutions depends on the stimulus velocities because of the asymmetric recurrent interactions in the network, and, therefore, they are suitable for modeling the activity of direction-selective neurons, as demonstrated by previous studies [6–8].

In contrast with these earlier studies, we are able to give an exact solution for the nonlinear network dynamics and to characterize the stability of the traveling pulse solutions. We find that the stability of such solutions depends on the stimulus speed, and can break down outside a certain regime of stimulus speeds. Outside this regime another class of solutions with characteristic spatiotemporal symmetry arises. Such solutions have been reported before in spiking networks [9–12] and in brain slices [13,14], and have been termed *lurching activity pulses*.

We find solutions with similar spatiotemporal characteristics in the absence of any spiking mechanism, self-organized by the interplay between the network dynamics and the incoming time-dependent stimulus. This solution type was observed in our simulations for different types of threshold nonlinearities and over a regime of different parameters.

The bifurcation that underlies the transition between form-stable and lurching wave solutions results from the essentially nonlinear properties of the network dynamics. For this reason, it is crucial that in our mathematical analysis we take the threshold nonlinearity of the neurons into account. This contrasts our work with previous studies that have presented approximate analyses of similar recurrent network models by applying methods from linear systems theory [6,8,15].

Our mathematical analysis extends and combines methods that have been presented in the literature before [16–20], and applies them to a new solution class. The characteristic instability and lurching solutions seem to be difficult to account for on the basis of the classical models for direction selectivity. This leads us to conclude that the existence of lurching activity pulses provides an experimentally testable prediction that is very specific for the explanation of direction selectivity by asymmetric lateral connections.

II. BASIC MODEL

Dynamic neural fields have been repeatedly proposed as models for the average behavior of a large ensemble of neurons [17,18,21–24]. The scalar neural activity distribution $u(x,t)$ characterizes the average activity at time t of an en-

*Electronic address: xhx@ai.mit.edu

semble of functionally similar neurons that code for stimulus feature x. Using a continuous approximation of biophysically spatially discrete neuronal dynamics, it is in some cases possible to treat the nonlinear neural dynamics analytically.

The field dynamics of the neural activation variable $u(x,t)$ of our model is described by

$$\tau\frac{\partial u(x,t)}{\partial t}+u(x,t)=\int_\Omega w(x-x')f(u(x',t))dx'+b(x,t). \tag{1}$$

The left side of this equation models a leaky integrator with a total input that is given by the right hand side of the equation. This input signal includes a feedforward input term $b(x,t)$ and a feedback term that integrates the recurrent contributions from other laterally connected neurons. The *interaction kernel* $w(x-x')$ characterizes the average synaptic connection strength between the neurons coding position x' and the neurons coding position x. f is the *activation function* of the neurons. This function is nonlinear and monotonically increasing. It introduces the nonlinearity that makes it difficult to analyze the network dynamics.

In the following we consider stimuli with a constant activity profile that move at a constant velocity v. We study how the solutions of the network dynamics, and, in particular, how their stability changes when the stimulus speed v is varied.

In the presence of a stimulus that moves with a constant velocity v, the mathematical description of the dynamics can be simplified by using a moving frame of coordinates by changing the spatial variable to $\xi=x-vt$. In this new frame the stimulus is stationary: $B(\xi)=b(x,t)$. With the activity in the new frame $U(\xi,t)=u(x,t)$ the dynamics is

$$\tau\frac{\partial U(\xi,t)}{\partial t}-\tau v\frac{\partial U(\xi,t)}{\partial \xi}+U(\xi,t) = \int_\Omega w(\xi-\xi')f(U(\xi',t))d\xi'+B(\xi). \tag{2}$$

A stationary solution in the moving frame has to satisfy

$$-\tau v\frac{dU^*(\xi)}{d\xi}+U^*(\xi)=\int_\Omega w(\xi-\xi')f(U^*(\xi'))d\xi' + B(\xi). \tag{3}$$

$U^*(\xi)$ corresponds to a traveling pulse solution with velocity v in the original static coordinates. Therefore, the traveling pulse solution driven by the moving stimulus can be found by solving Eq. (3). The stability of the traveling pulse can be studied by perturbing the stationary solution in Eq. (2).

The neural field dynamics Eq. (2) is a nonlinear integro-differential equation. In most cases an analytic treatment of such equations is impossible. In this paper, we consider two biologically inspired special cases for which an analytical solution can be found. For this purpose we consider only one-dimensional neural fields and assume that the nonlinear activation function f is either a step function, or a linear threshold function.

III. STEP ACTIVATION FUNCTION

We first consider the step activation function $f(z)=\Theta(z)$ where $\Theta(z)=1$ when $z>0$ and zero otherwise. This form of activation function approximates the activities of neurons that, by saturation, are either active or inactive. For the one-dimensional case, we assume that only a single stationary excited regime with $[U^*(\xi)>0]$ exists and is located between the points (ξ_1^*,ξ_2^*). The validity of this assumption depends on the shape of the input $B(\xi)$ and the interaction kernel w [34]. Only neurons inside this regime contribute to the integral. Moreover, because f is constant in this regime this contribution only depends on the boundary values ξ_1^* and ξ_2^*. Accordingly, the spatial shape $U^*(\xi)$ of the stationary solution obeys the ordinary differential equation,

$$-\tau v\frac{dU^*(\xi)}{d\xi}+U^*(\xi)=W(\xi-\xi_1^*)-W(\xi-\xi_2^*)+B(\xi), \tag{4}$$

where the function $W(\cdot)$ satisfies $W'(x)=w(x)$. The solution of the last equation can be found by treating the boundaries ξ_1^* and ξ_2^* as fixed parameters and solving Eq. (4). To facilitate notation we define the following integral operator O with parameter $\alpha\neq 0$:

$$O[g(z);\alpha]\equiv\int_{z_0}^{z} g(m)\exp[(z-m)/\alpha]dm, \tag{5}$$

where $z_0=-\infty$ for $\alpha<0$ and $z_0=+\infty$ for $\alpha>0$. Using this operator we define two functions $F(z)=O[W(z);\tau v]/(-\tau v)$ and $G(z)=O[B(z);\tau v]/(-\tau v)$. The solution of Eq. (4) can be written with these functions in the form

$$U^*(\xi)=F(\xi-\xi_1^*)-F(\xi-\xi_2^*)+G(\xi). \tag{6}$$

For the boundary points, $U^*(\xi_1^*)=U^*(\xi_2^*)=0$ must be satisfied, leading to the transcendental equation system,

$$-F(0)+F(\xi_1^*-\xi_2^*)=G(\xi_1^*), \tag{7}$$

$$F(0)-F(\xi_2^*-\xi_1^*)=G(\xi_2^*), \tag{8}$$

from which ξ_1^* and ξ_2^* can be determined. To be consistent with our initial assumption, it has to be verified that the solution $U^*(\xi)$ indeed has only one excited regime between ξ_1^* and ξ_2^*.

A. Stability of the traveling pulse solution

The stability of the traveling pulse solution can be analyzed by perturbing the dynamics around the stationary solution in the moving frame. To consider the step threshold nonlinearity in the dynamics, we perturb both the wave form and the boundary points. In addition, the perturbation of the

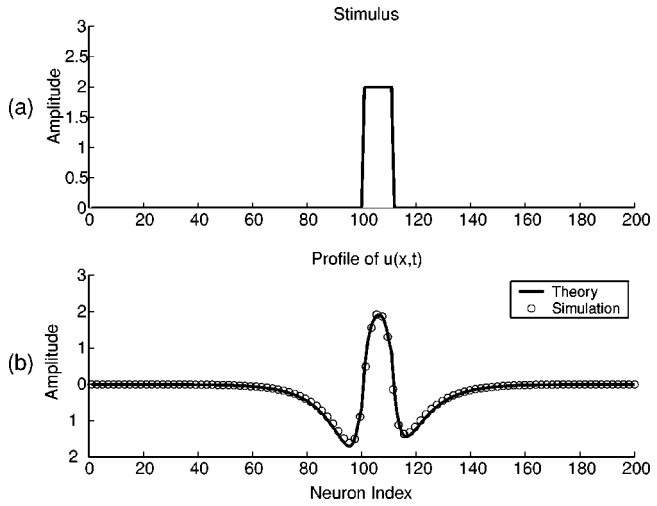

FIG. 1. Stimulus and activity profile in the step activation function model. Panel (a) shows the stimulus, and panel (b) the activity $m(x,t)$ at the time t for the traveling pulse solution. The solid line in (b) shows the result from the calculation, while the circles indicate the numerical simulation results. The interaction kernel used in this simulation was $w(x)=a_e\exp(-k_e|x-x_0|)-a_i\exp(-k_i|x-x_0|)$ with $a_e=1$, $a_i=5$, $k_e=0.42$, $k_i=0.1$, and $x_0=3$. The stimulus was a moving bar with width $d=10$ and amplitude $h=2$. Notice that the activity profile $u(x,t)$ has only a single excited regime.

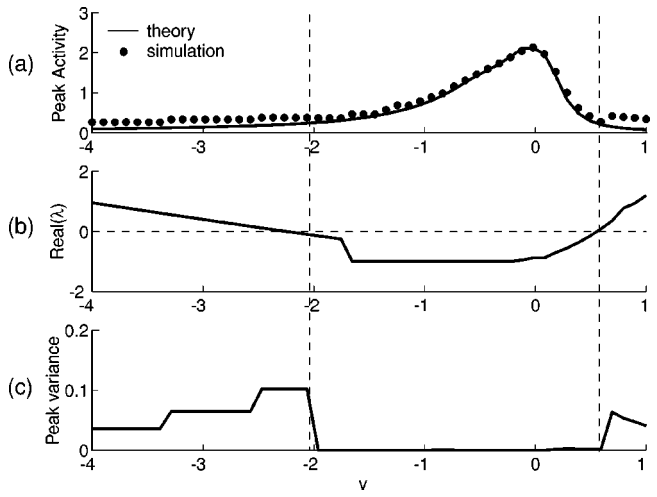

FIG. 2. Traveling pulse solution and its stability in the step activation function model. Panel (a) shows the velocity tuning curves and the peak amplitude of the traveling pulse. The solid lines indicate the theoretical results, while the dots signify the numerical simulation results. The velocity v is normalized by the time constant of the dynamics in the unit of rad/τ. Panel (b) shows the largest real parts of the eigenvalue λ obtained by solving Eq. (9) numerically. Only solutions corresponding to the negative values of this function are form stable. Panel (c) plots the variations of the peak amplitude of the pulse. A variance that deviates significantly from zero signifies a loss of stability of the traveling pulse solutions. The results are consistent with analysis of the eigenvalues in panel (b). Also notice that in panel (a) the theoretical peak amplitude fits well the simulation results only inside the stable regime.

boundary points can be related to the perturbation of the wave form at the boundary points. Based on this, we determine the eigenvalue equation for the linearized perturbation dynamics,

$$[K(0)-c_1^*(1+\tau\lambda)][K(0)+c_2^*(1+\tau\lambda)] = K(\xi_1^*-\xi_2^*)K(\xi_2^*-\xi_1^*), \tag{9}$$

where $c_i^*\equiv dU^*(\xi_i)/d\xi$ for $i=1,2$, and the function $K(\cdot)$ is defined as

$$K(z)\equiv O[w(z);\tau v/(1+\tau\lambda)](1+\tau\lambda)/(-\tau v).$$

From this equation eigenvalues λ can be found numerically. The traveling pulse solution is asymptotically stable only if the real parts of all eigenvalues λ are nonpositive. The detailed derivation of the eigenvalue equation is shown in the Appendix.

B. Simulation results of step activation function model

In the previous analysis the only restriction for the interaction kernel was that it should allow solutions with a single excited regime. To test our mathematical results we simulated the model using an interaction function that was given by a difference of two exponential functions, simulating a receptive field with asymmetric local excitation and center-surround inhibition. Lateral connectivity of similar type, but typically symmetric with respect to the receptive field center, has been used in many models for short range interactions in the visual cortex. The advantage of using exponentials is that one can carry out the integration in Eq. (5) explicitly, which simplifies the subsequent calculations considerably.

We simulated the dynamics numerically and compared the results with the results from the mathematical analysis. The kernel had the following form:

$$w(x)=a_e\exp(-k_e|x-x_0|)-a_i\exp(-k_i|x-x_0|),$$

where a_e and a_i are the amplitudes of excitation and inhibition. x_0 is an offset that causes the network to be asymmetric and induces the direction sensitivity.

As stimulus $b(x,t)$ we used a moving ''bar'' with constant width and amplitude. Figure 1 plots a snapshot of the activity profile of $u(x,t)$ and stimulus $b(x,t)$ at a time t in the regime where the traveling pulse solution is stable. On top of the analytically calculated profile $u(x,t)$, we also plotted simulation results, which show good consistency with the theory.

We also determined the peak activities of $u(x,t)$ as function of the stimulus speed. The peak amplitude as a function of the speed is shown in Fig. 2. Panel (a) shows the speed tuning curve plotted as the dependence of the peak activity of the traveling pulse as a function of the stimulus velocity v. The solid line indicates the results from the theoretical solution and the dots indicate the simulation results. Panel (b) shows the maximum of the real parts of the eigenvalues obtained from Eq. (9). For stimulus velocities outside a certain range this maximum becomes positive indicating a loss of stability of the form-stable solution. To verify this result we calculated also the variability of the peak activity over time after excluding the initial transients from the simulations.

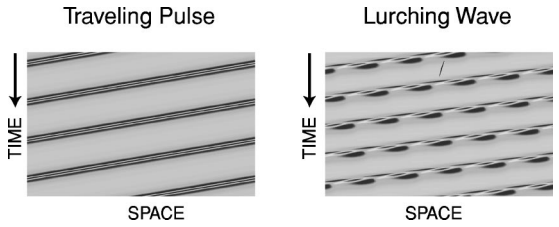

FIG. 3. Traveling pulse and lurching wave in step activation function model. The color-coded plots show the spatial-temporal evolution of the activity $u(x,t)$. The left panel shows the propagation of the form-stable peak over time. The right panel shows the lurching activity wave that arises when stability is lost.

Panel (c) shows the variations as function of the stimulus velocity. At the velocities for which the eigenvalues indicate a loss of stability the variability of the amplitudes suddenly increases. This indicates that the stationary solution is not time independent any more, consistent with our interpretation that the form-stable solution loses stability.

An interesting observation is illustrated in Fig. 3 that shows the space-time evolution of the activity. The left panel shows the propagation of the form-stable traveling pulse for medium stimulus speeds. The right panel shows the solution that arises when stability is lost. This solution is characterized by a characteristic spatiotemporal periodicity that is defined in the moving coordinate system by $U(y+mL_0,t+nT_0)=U(y,t)$, where L_0 and T_0 are constants that depend on the network dynamics. Solutions of similar type have been described before in different contexts, such as in brain slice experiments [13,14] and in studies with spiking networks without time-dependent input signals. These solutions have been termed ''lurching waves'' because of the periodic discontinuity of the spatiotemporal evolution of the neural activity [10,11,25].

We have shown here only the comparison between theory and simulation for exponential interaction kernels and localized bar stimuli. However, we found in additional simulation studies that lurching activity waves arise very robustly for this type of networks also for other forms of interaction kernels or input signals. Further evidence for the robustness of the phenomenon of lurching waves is provided in the following by a demonstration that the same phenomenon arises also for another type of threshold function.

IV. LINEAR THRESHOLD MODEL

We also considered a model with an activation function f that had the form of a linear threshold, i.e., $f(z)=[z]^+=\max\{z,0\}$. Linear threshold models of similar type have been used before in a variety of neural modeling studies [22,18,26]. It has been argued that firing rates of neurons above threshold typically vary linearly with the stimulus strength. Moreover, neurons normally operate far below their saturation levels. Therefore, a linear threshold characteristic might approximate the activation function relatively well (cf., e.g., [27]). To further simplify the model, we consider a ring network with periodic boundary condition on the interval $\Omega=[-\pi,\pi)$.

The ring network dynamics can be written as

$$\tau\frac{\partial}{\partial t}m(\theta,t)+m(\theta,t)=\left[\int_{-\pi}^{\pi}w(\theta-\theta')m(\theta',t)(2\pi)^{-1}\,d\theta'+b(\theta,t)\right]^+, \tag{10}$$

where $b(\theta,t)$ is the time-dependent feedforward input.

The network in this form can be transformed to the network in the standard form that is given by Eq. (1) by a change of variables and by transforming the stimulus distribution. Defining the total network input $u(\theta,t)$ by

$$u(\theta,t)\equiv\int_{-\pi}^{\pi}w(\theta-\theta')m(\theta',t)(2\pi)^{-1}\,d\theta'+b(\theta,t), \tag{11}$$

we obtain the following dynamics for u:

$$\tau\frac{\partial}{\partial t}u(\theta,t)+u(\theta,t)=\int_{-\pi}^{\pi}w(\theta-\theta')[u(\theta',t)]^+(2\pi)^{-1}\,d\theta'+\tilde{b}(\theta,t), \tag{12}$$

where the transformed stimulus $\tilde{b}(\theta,t)$ obeys the partial differential equation, $\tilde{b}(\theta,t)=\tau\partial b(\theta,t)/\partial t+b(\theta,t)$.

For convenience, in the following discussions we use Eq. (10) for the analysis of the system dynamics. As in the previous model, the stimulus moves with a constant velocity $b(\theta,t)=B(\theta-vt)$. Again, we analyze traveling pulse solutions that are driven by the stimulus, and their stability.

A. General solutions and stability analysis

Because the activation function has linear threshold characteristics, inside the excited regime for which the total input $[u(\theta,t)>0]$ is positive the system is linear. One approach to solve this dynamics is, therefore, to find the solutions to the differential equation assuming the boundaries of the excited regime are given. The conditions at the boundaries lead to a set of self-consistent equations for the solutions to satisfy, from which the boundaries can be determined.

By denoting activities in moving coordinates as $M(\theta-vt,t)=m(\theta,t)$, the dynamics can be written as

$$\tau\frac{\partial}{\partial t}M(\theta,t)-\tau v\frac{\partial}{\partial\theta}M(\theta,t)+M(\theta,t)=\left[\int_{-\pi}^{\pi}w(\theta-\theta')M(\theta',t)(2\pi)^{-1}\,d\theta'+B(\theta)\right]^+. \tag{13}$$

Supposing the excited regime is $\theta\in[\theta_1(t),\theta_2(t)]$, we solve the dynamics by Fourier transforming the above equation in the spatial domain $[-\pi,\pi)$. Let

$$\hat{m}_n(t)=\int_{-\pi}^{\pi} M(\theta,t)\exp(in\theta)(2\pi)^{-1}\,d\theta$$

and

$$\hat{w}_n=\int_{-\pi}^{\pi} w(\theta)\exp(in\theta)(2\pi)^{-1}\,d\theta.$$

Then in terms of these Fourier modes, the dynamics can be written as

$$\tau\dot{\hat{m}}_n+(1+i\tau v n)\hat{m}_n=\sum_l C_{nl}\hat{m}_l+\hat{b}_n,$$

for $n=0,\pm 1,\ldots,$ with

$$C_{nl}=(2\pi)^{-1}\hat{w}_l[(\theta_2-\theta_1)\delta_{nl}-i(e^{i(n-l)\theta_2}-e^{i(n-l)\theta_1})\times(n-l)^{-1}(1-\delta_{nl})],$$

$$\hat{b}_n=\int_{\theta_1}^{\theta_2} B(\theta)\exp(in\theta)(2\pi)^{-1}\,d\theta.$$

where δ_{nl} is the Kronecker delta defined as having the value one when $n=l$, and zero when $n\neq l$.

Therefore, the stationary solution in moving coordinates is

$$\hat{\mathbf{m}}^*=(I+i\tau v K-C)^{-1}\hat{\mathbf{b}}, \tag{14}$$

where matrix K is defined as the diagonal matrix $K\equiv\mathrm{diag}([0,1,-1,2,-2,\ldots])$. The components of the vector $\hat{\mathbf{m}}$ are $\hat{m}_n$, and those of $\hat{\mathbf{b}}$ are $\hat{b}_n$. The total input for the stationary solution in the moving frame can then be written as

$$U^*(\theta)=\sum_n \exp(-in\theta)\sum_l C_{nl}\hat{m}_l^*+B(\theta), \tag{15}$$

which has to satisfy the two boundary conditions $U^*(\theta_1)=U^*(\theta_2)=0$. From these two equations the stationary values of θ_1 and θ_2 can be determined.

The stability of this traveling pulse solution can be analyzed by linear perturbation theory. Note that the perturbations of the boundary points will not contribute to the linearized perturbed dynamics because the contribution from this perturbation is $\delta\theta_i U^*(\theta_i)=0$ for $i=1,2$. Therefore, the linearized perturbation dynamics can be fully characterized by the perturbed Fourier modes with fixed boundaries. Hence, the stability of the traveling pulse solution is determined by the eigenvalues of the matrix $A=-(I+i\tau v K-C)$. If the maximum of the real parts of the eigenvalues of A is negative, then the stimulus locked traveling pulse is stable.

B. Linear threshold network with simple kernels

The general solution introduced above requires the solution of a system of equations. In practice, the Fourier series has to be truncated in order to obtain a finite number of Fourier components at the expense of an approximation error.

Next we use a simple model that contains only the first two Fourier components in both the interaction kernel and the input distribution. We modify the model by introducing asymmetry into the interaction kernel, and study how the network activity changes as a function of the stimulus velocity. For this model, a closed form solution and stability analysis are presented that provides an insight into some rather general properties of linear threshold networks.

The interaction kernel and feedforward input are taken to be of the following form:

$$w(\theta)=J_0+J_1\cos(\theta+\beta), \tag{16}$$

$$b(\theta,t)=C\{1-\epsilon+\epsilon\cos[\theta-\theta_0(t)]\}-T, \tag{17}$$

where the variable β makes the interaction asymmetric. In the input, the threshold term T is subtracted, and $\theta_0(t)=vt$ is the input's peak location. This model was introduced by Hansel and Sompolinsky in their model of cortical orientation selectivity [18], with $w(\theta)$ being symmetric and b being static.

Since the interaction kernel and feedforward input involve only the first two Fourier components, the Fourier transform method presented in the previous section can be simplified significantly. As a consequence, the dynamics of the network can be studied in terms of the first two Fourier components of $M(\theta,t)$, namely, $\hat{m}_0(t)$ and $\hat{m}_1(t)$. Next we present the analysis, following similar treatments of Hansel and Sompolinsky [18].

The first Fourier component $\hat{m}_0(t)$ is a real number representing the mean of the neural activities, which is denoted by $r_0(t)$ in the following. The second Fourier component $\hat{m}_1(t)$ is a complex number. Let us denote the amplitude of $\hat{m}_1(t)$ by $r_1(t)$. Therefore, in summary we have

$$r_0(t)=\hat{m}_0(t)=\int_{-\pi}^{\pi} m(\theta,t)(2\pi)^{-1}\,d\theta, \tag{18}$$

$$r_1(t)=|\hat{m}_1(t)|=\int_{-\pi}^{\pi} m(\theta,t)\exp[i\{\theta-\Psi(t)\}](2\pi)^{-1}\,d\theta, \tag{19}$$

where the phase $\Psi(t)$ is used to make the right hand side of the equation being a real number.

In terms of the Fourier components, the total input in Eq. (10) can be written as

$$I(\theta,t)=\int_{-\pi}^{\pi} w(\theta-\theta')m(\theta',t)(2\pi)^{-1}\,d\theta'+b[\theta-\theta_0(t)]$$
$$=I_0(t)+I_1(t)\cos(\theta-\Phi), \tag{20}$$

where $I_0(t)$ and $I_1(t)$ are defined as

$$I_0(t)=C(1-\epsilon)+J_0 r_0(t)-T, \tag{21}$$

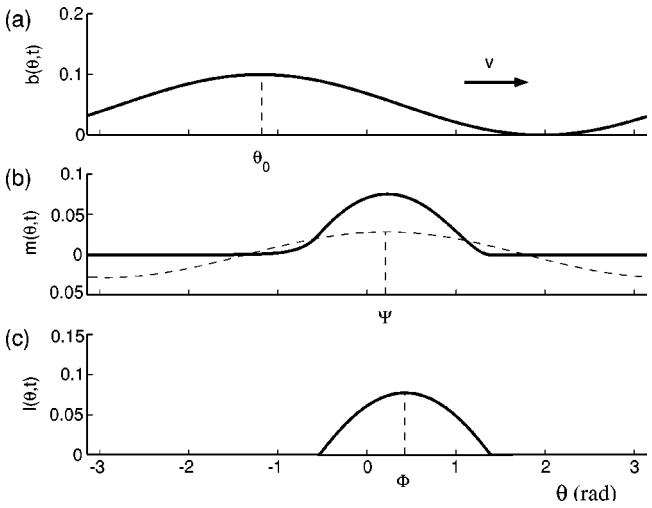

FIG. 4. Traveling pulse for the linear threshold model with a simple periodic kernel [Eq. (16)]. Panel (a) shows the stimulus with a moving peak centered at θ_0. The activation profile $m(\theta,t)$ is shown in panel (b). The dashed line indicates its first order Fourier component with a maximum at Ψ. Panel (c) shows the profile of the total input $I(\theta,t)$. The phase variable Φ is defined by the peak location of the total input.

$$I_1(t)=\epsilon C\cos[\theta_0(t)-\Phi]+J_1 r_1(t)\cos(\Psi-\Phi-\beta). \tag{22}$$

Here, the phase variable $\Phi(t)$ represents the location for the peak of the total input, that is, $\Phi(t)=\mathrm{argmax}_\theta\, I(\theta,t)$, which should satisfy

$$\epsilon C\sin(\Psi-\theta_0(t))+J_1 r_1\sin(\Phi-\Psi+\beta)=0. \tag{23}$$

Figure 4 shows a snapshot of the network activity $m(\theta,t)$, the total input $I(\theta,t)$, and the stimulus $b(\theta,t)$ at the time t. Three phase variables are indicated in the figure, with θ_0, Ψ, and Φ being the peak location of the input, the first Fourier mode, and the total input $I(\theta,t)$, respectively.

To write down the dynamics in terms of these Fourier components, we need one more step to take care of the rectification nonlinearity. Suppose there is only a single excited interval $\theta\in(\Phi-\theta_c,\Phi+\theta_c)$ in which the total input $I(\theta,t)$ is positive. From Eq. (20), the critical width can be determined as $\theta_c=\arccos(-I_0/I_1)$. Using θ_c, the dynamics can be rewritten as

$$\tau\frac{\partial}{\partial t}m(\theta,t)+m(\theta,t)=I_1(t)[\cos(\theta-\Phi)-\cos(\theta_c)]^+. \tag{24}$$

Fourier transforming the above equation, we derive the dynamics of the Fourier components,

$$\tau\dot{r}_0=-r_0+I_1(t)f_0(\theta_c), \tag{25}$$

$$\tau\dot{r}_1=-r_1+I_1(t)f_1(\theta_c)\cos(\Phi-\Psi), \tag{26}$$

$$\tau r_1\dot{\Psi}=I_1(t)f_1(\theta_c)\sin(\Phi-\Psi), \tag{27}$$

where two functions $f_0(\theta_c)$ and $f_1(\theta_c)$ are defined as

$$f_0(\theta_c)=\pi^{-1}[\sin(\theta_c)-\theta_c\cos(\theta_c)],$$

$$f_1(\theta_c)=(2\pi)^{-1}[\theta_c-\sin(2\theta_c)/2].$$

Interestingly, introducing the time-dependent input and asymmetric connections does not change the principle form of the Fourier component dynamics compared with the case with static inputs and symmetric connections [18]. Instead, the changes only appear inside $I_1(t)$ [see Eq. (22)]. This property is very helpful for the analysis of the dynamics of this system.

Similarly, we can derive the dynamics of the Fourier components with orders higher than two. But fortunately, the dynamics in Eqs. (25)–(27) is independent of these higher order components. Moreover, it can be shown that if the dynamics in Eqs. (25)–(27) is stable, the dynamics of the higher order Fourier components is stable as well. Therefore, the stability of these three-dimensional dynamics fully characterizes that of the neural field Eq. (24).

C. Traveling pulse solutions

A traveling pulse solution corresponds to a stationary solution in the moving frame. Therefore, $\dot{r}_0=\dot{r}_1=0$ and $\dot{\Psi}=v$, which lead to

$$r_0=I_1 f_0(\theta_c),$$

$$r_1=I_1 f_1(\theta_c)\cos(\Phi-\Psi),$$

$$\tau v=\tan(\Phi-\Psi).$$

Suppose that θ_c is given. From the above equations, the Fourier components r_0 and r_1 can be derived as

$$r_0=[(1-\epsilon)C-T]f_0(\theta_c)[-J_0 f_0(\theta_c)-\cos(\theta_c)]^{-1}, \tag{28}$$

$$r_1=[(1-\epsilon)C-T]\cos(\Delta)f_1(\theta_c)[-J_0 f_0(\theta_c)-\cos(\theta_c)]^{-1}, \tag{29}$$

where the variable $\Delta\equiv\Phi-\Psi=\mathrm{atan}(\tau v)$. Subsequently, I_0 and I_1 can be determined from Eqs. (21) and (22). Substituting them into Eq. (23) leads to

$$1-\Gamma^{-1}=[J_0 f_0(\theta_c)+\cos(\theta_c)][J_1^2 f_1^2(\theta_c)\cos^2(\Delta) - 2J_1 f_1(\theta_c)\cos(\Delta)\cos(\Delta+\beta)+1]^{-1/2}, \tag{30}$$

where $\Gamma\equiv\epsilon C/(C-T)$ represents the contrast of the stimulus. From this equation, the critical width θ_c can be found, using numerical methods. Consequently, the values of r_0 and r_1 can be determined.

D. Existence of traveling pulse solutions

The critical width θ_c must satisfy Eq. (30). The existence of traveling pulse solutions depends on whether θ_c exists for

a given stimulus velocity v. It is possible that θ_c does not exist for a particular range of v. Next we characterize the conditions on v for the existence of a traveling pulse solution.

Let $B=[J_0 f_0+\cos(\theta_c)]\Gamma/(\Gamma-1)$. Then, Eq. (30) can be rewritten as

$$[J_1 f_1 \cos(\Delta)-\cos(\Delta+\beta)]^2=B^2-\sin^2(\Delta+\beta).$$

Therefore, for a solution θ_c to exist, we must have $|\sin(\Delta+\beta)|\leqslant B$. Dividing both sides by $\cos(\beta)\cos(\Delta)$, we derive the condition that v has to satisfy for the existence of θ_c

$$|v-v^*|\leqslant \frac{\sqrt{1+\tau^2 v^2}}{\tau\cos(\beta)}B, \tag{31}$$

where $v^*\equiv-\tan(\beta)/\tau$.

The above equation cannot be used to determine the v for which a traveling pulse solution arises, since the right hand side of the equation depends on the unknown variable θ_c. However, it gives some general characterizations about the admissible range of v.

For example, the limit for the stimulus contrast $\Gamma\to 0$ implies the only admissible $v=v^*$, which means that the traveling pulse solution has a unique velocity v^* that is independent from the stimulus, and determined only by the network dynamics. Solutions of this type have been analyzed before for networks with saturating threshold functions in Ref. [28]. In this case the traveling pulse solution is caused purely by the asymmetric structure of the network, parametrized here by the variable β. When the stimulus is not uniform, the traveling pulse solution exists only when the stimulus velocity is not too different from the intrinsic velocity v^*. The smaller the contrast B, the smaller is the range of stimulus speeds v for which a traveling pulse solution exists. This range is also influenced by the time constant τ. Smaller τ lead to a larger velocity range.

E. Optimal velocity

The network presented here is asymmetric, and has its own intrinsic velocity v^* determined by the asymmetry parameter β. When the network is driven by the stimulus moving at different velocities the amplitude of the solution is modulated as a function of the velocity. This dependency defines the *velocity tuning curve*, which can be measured in physiological experiments. To characterize the velocity tuning curve fully in this network is not easy since θ_c can only be determined numerically. We focus, therefore, on finding the optimal stimulus velocity that leads to the maximal mean activity r_0.

Note that r_0 in Eq. (28) only depends on θ_c, but not directly on v. Furthermore, r_0 depends on θ_c only through $\cos(\theta_c)/f_0(\theta_c)$ as

$$r_0(\theta_c)=[(1-\epsilon)C-T][-J_0-\cos(\theta_c)/f_0(\theta_c)]^{-1}.$$

For $\theta_c\in[0,\pi]$ it is easy to check that $f_0(\theta_c)$ is monotonically increasing, and consequently $\cos(\theta_c)/f_0(\theta_c)$ is monotonically decreasing. Overall, $r_0(\theta_c)$ is a monotonically decreasing function of θ_c. Therefore, the optimal velocity v^m for which r_0 is maximal corresponds to the smallest value of θ_c in Eq. (30), that is $v^m\equiv\mathrm{argmax}_v\, r_0(\theta_c(v))=\mathrm{argmin}_v\,\theta_c(v)$.

Taking the derivative with respect to v on both sides of Eq. (30) and using the condition $d\theta_c(v^m)/dv=0$ yields

$$v^m=-\frac{J_1 f_1\sin(\beta)}{\tau(1-B^2)}.$$

When the stimulus contrast is small, $\Gamma\ll 1$, we have $B\ll 1$ and $J_1 f_1\approx 1/\cos(\beta)$. Substituting this result into the above equation, we find for weak stimulus contrast $v^m\approx v^*$. This implies that the optimal velocity for which the mean activity is maximal is the intrinsic velocity. This is a nice property in the sense that it relates the optimal stimulus velocity to the network structure. By changing the asymmetry parameter β, the network can have different preferred velocities. Notice that the approximate equality between the optimal v^m and the intrinsic v^* holds only if the stimulus contrast is low.

F. Stability analysis of the traveling pulse

A stability analysis can be carried out by perturbing the dynamics of the Fourier components in Eqs. (25)–(27). The final linearized perturbation dynamics is shown in the Appendix. In the case when $\epsilon C\ll 1$, the perturbed dynamics can be simplified into

$$\tau\delta\dot{r}_0=(\pi^{-1}J_0\theta_c-1)\delta r_0+\pi^{-1}J_1\sin(\theta_c)\delta r_1, \tag{32}$$

$$\tau\delta\dot{r}_1=\pi^{-1}\cos(\beta)\sin(\theta_c)J_0\delta r_0+\{-1+(2\pi)^{-1}J_1[\theta_c+\sin(2\theta_c)/2]\cos(\beta)\}\delta r_1. \tag{33}$$

G. Simulation results for the linear threshold model

Figure 5 shows the comparison between the results from the mathematical analysis and the simulations. Panel (a) shows the speed tuning curve plotted as values of r_0 and r_1 with respect to different stimulus velocities v. The solid and dashed lines indicate calculation results, and the dotted lines represent those from numerical simulations. Panel (b) shows the largest real part of the eigenvalues of the stability matrix obtained by linearizing the three-dimensional Fourier component dynamics around the stationary solution as described in the preceding section. For stimulus velocities outside a certain range, the maximum of the real parts of the eigenvalues becomes positive indicating a loss of stability of the form-stable solution. To verify this result we calculated the variations of r_0 and r_1 over time in the simulation. Panel (c) shows the variations as a function of the stimulus velocity. At the velocities for which the eigenvalues indicate a loss of stability the variations of r_0 and r_1 suddenly increase, consistent with our interpretation.

Like the results shown before for the step function model (Fig. 3), Fig. 6 illustrates the space-time evolution of the

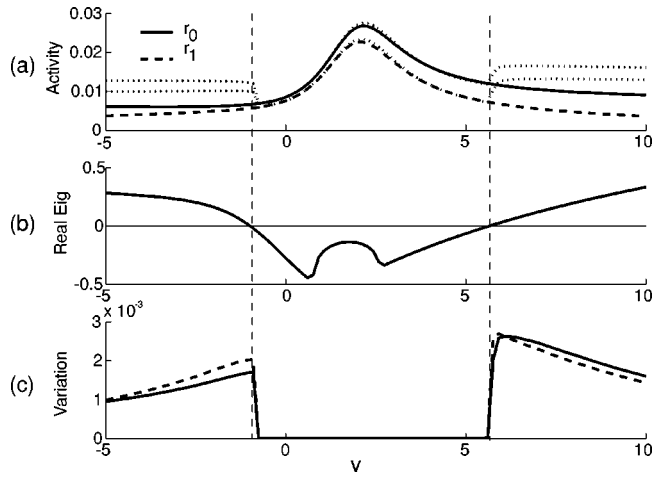

FIG. 5. Traveling pulse solution and its stability in the linear threshold model. Panel (a) shows the velocity tuning curves of r_0 and r_1. The dotted lines indicate numerical simulation results, while solid and dashed lines are the results from our analytical solution. The theoretical results fit well the simulation results in the range of velocity between the two vertical dashed lines. Panel (b) shows the maximum of the real parts of eigenvalues of the stability matrix obtained by perturbing the dynamics around the stationary solution. For stimulus velocities outside a certain range this value becomes positive, indicating a loss of stability of the form-stable solution. Panel (c) shows the variations of r_0 (solid curve) and r_1 (dashed curve) over time determined from the simulation. A nonzero variance signifies a loss of stability for the traveling pulse solution, consistent with the eigenvalue analysis in panel (b). The velocity v is normalized by the time constant of the dynamics in the unit of rad/τ. Parameters used are $C=5$, $\epsilon=0.01$, $T=4.9$, $J_0=-9.8$, $J_2=13.5$, and $\beta=0.46$.

activity. The left panel shows the propagation of the form-stable peak over time, whereas the right panel shows the solution that arises when stability is lost. Like those in the model with a step threshold, lurching activity pulses arise for a whole regime of different parameters for networks that show substantially direction selective behavior.

The phase diagram of the form-stable traveling pulse solution is plotted in Fig. 7, where we show the range of stimulus velocity for a stable traveling pulse as the asymmetry parameter β, and consequently the intrinsic velocity $[v^*=-\tan(\beta)/\tau]$, changes. The stable region for v is typically located around the intrinsic velocity v^*.

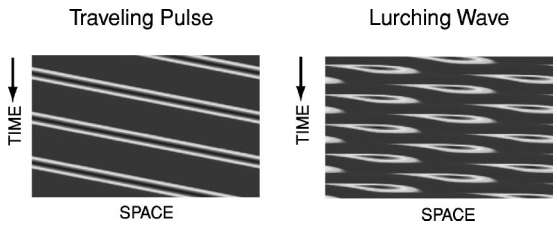

FIG. 6. Traveling pulse and lurching wave in the linear threshold model. Shown here is a color-coded plot of spatial-temporal evolution of the activity $m(x,t)$. The left panel shows the propagation of the form-stable peak over time, whereas the right panel shows the lurching activity wave that arises when stability is lost.

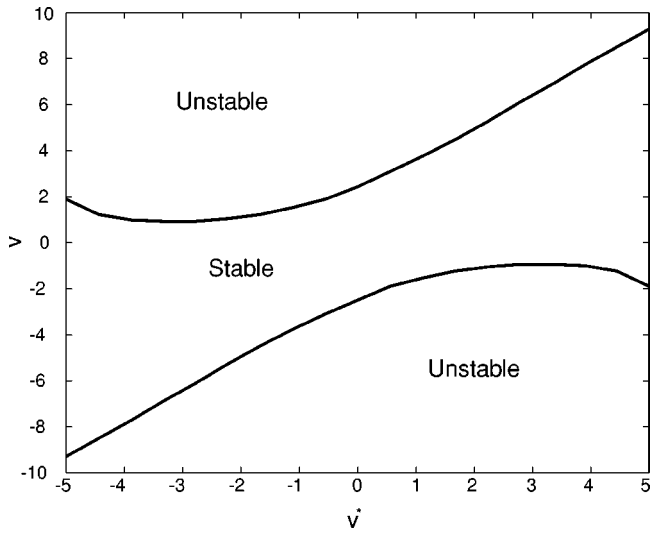

FIG. 7. Stable regime of traveling pulse solutions. Shown here is the regime velocities v for which a stable traveling pulse solution arises as the intrinsic velocity v^* changes. The intrinsic velocity v^* depends on the asymmetry variable β of the interaction kernel.

So far, we have shown the traveling pulse and lurching wave solutions in models with step threshold and linear threshold activation functions. The development of direction selectivity of the travel pulse solutions among certain velocity range and loss of stability when outside the range are not confined only to these two types of models. To demonstrate this, we simulate the dynamics Eq. (1) with a sigmoidal shaped activation function and an asymmetric interaction kernel. Again, we observe the tuning of neural activities to input velocities, and the bifurcation of traveling pulse solutions to lurching waves when the velocity of the input is outside a certain range (Fig. 8).

V. CONCLUSION

In this paper we have presented a mathematical analysis of a class of models that account for the direction selectivity by asymmetric lateral connections between cortical neurons. Given the large number of recurrent connections in the visual cortex, it seems plausible that lateral connections play an important role for the realization of direction selectivity [6,7]. Contrasting with earlier works on such models [8,15], we have presented a mathematical analysis of the full nonlinear dynamics of such networks that takes the nonlinear response functions of the neurons into account.

One result from our analysis is that such recurrent models, for a certain regime of stimulus speeds, have traveling pulse solutions that are form stable and move with the same speed as the stimulus. We have termed such solutions *stimulus-locked traveling pulses*. In the stationary state, these solutions have space-time characteristics that is also compatible with other models for direction selectivity, e.g., motion energy models with feedforward structure, or models with linear feedback. In particular, the recurrent mechanism that we analyzed can account for biologically realistic degrees of velocity tuning of cortical neurons [8]. The preferred speed of the neurons in such recurrent models is determined by the

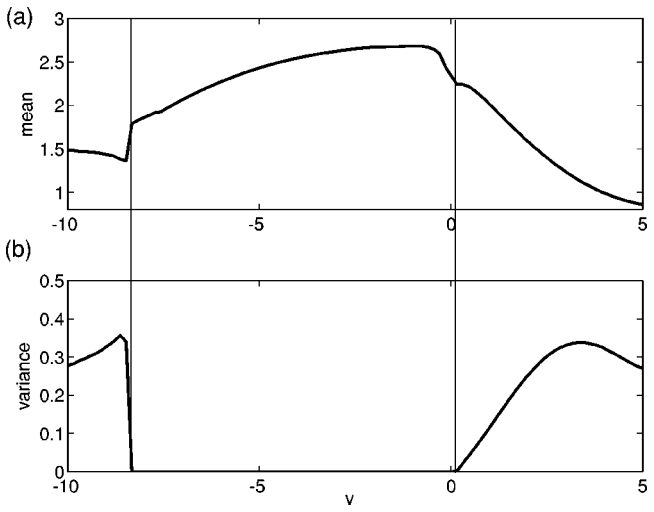

FIG. 8. Traveling pulse solution and its stability with a sigmoidal shaped activation function. Panel (a) shows that mean peak activity of the moving solutions and panel (b) plots the variations of the solution averaged over time. The traveling pulse solution is stable only for velocities between the two vertical lines. The velocity v is normalized by time constant τ in the unit of rad/τ. The activation function used is $f(x)=1/[1+\exp(-2x)]$. The interaction kernel is the difference of two Gaussian functions, but with the center shifted, $w(x)=A_e\exp[-(x-\mu)^2/(2\sigma_e^2)]-A_i\exp[-(x-\mu)^2/(2\sigma_i^2)]$ with $\sigma_e=0.08$, $\sigma_i=1$, $A_e=62$, $A_i=37$, and $\mu=0.05$. The input used is a rectified bump $b(\theta,t)=7\exp\{[\cos(\theta-vt)-2]^+\}$.

network structure. For example, we show that for the model with linear threshold activation function, the preferred speed for input signals with small contrast is close to the equilibrium speed of the self-generated traveling pulse solution in the absence of a time-dependent stimulus. The speed tuning in the nonlinear model that we analyzed arises because, for sufficiently strong interaction, the network tends to stabilize a traveling peak solution that ''locks'' to the moving activity peak of the stimulus. This solution becomes unstable if this locking is lost.

Our stability analysis shows that the traveling pulse solution is stable only within a certain regime of stimulus speeds. At the borders of this regime a bifurcation arises and the stimulus-locked solution becomes unstable. Such speed-dependent bifurcations cannot arise in the classical feedforward models, and in networks with linear feedback. For such networks the solutions are either always stable, or the network is unstable.

An important observation in our simulations is that the loss of stability of the stimulus-locked solution is frequently accompanied by the formation of *lurching activity pulses*. Lurching activity has been described by different other authors in brain slices [13,14], and in artificial spiking networks without time-dependent inputs [11,12]. Our simulation results imply that spiking neurons are not necessary for the generation of lurching activity waves if a moving stimulus is present. Such lurching waves cannot be produced by a feedforward network, in which the output of the network is always phase locked to the stimulus. Moreover, there is no stability issue in feedforward networks. Therefore, the bifurcation observed in recurrent networks cannot appear in feedforward networks. In models with linear feedback, oscillations of the activity could potentially be obtained, e.g., if the network contains multiple neuron populations that are connected by excitatory connections. Still it would be difficult to account for the speed dependence of the bifurcation.

With respect to the mathematics, we have tried to characterize a class of solutions of spatially continuous neural networks that is different from solutions have been analyzed in previous work that apply similar mathematical methods. By the presence of a time-dependent stimulus, the stimulus-locked traveling pulse solution is different from the stable stationary solutions of networks with static inputs that have been repeatedly analyzed in the literature (e.g. [16,17,19,21,29]). The stimulus-locked solution is also different from self-generated traveling waves or pulses that have been studied in different contexts [28]. For such solutions the pulse propagates with an equilibrium speed that is specified by the network dynamics, whereas for the stimulus-locked traveling pulse solution the propagation speed is given by the stimulus. At least for the linear threshold model with small contrast, the speed regime for which a stimulus-locked traveling pulse solution exists is, however, in a neighborhood of the optimal speed with which a self-generated pulse would propagate in the absence of a time-dependent stimulus. The proposed recurrent mechanism for direction selectivity exploits a kind of ''resonance'' between the tendency of the network to stabilize a traveling pulse solution with characteristic speed and the incoming time-dependent stimulus activity.

We conclude from our analysis that the observation of lurching activity waves in populations of direction-selective neurons in the visual cortex would be a strong indicator for the relevance of the recurrent mechanism for direction selectivity that we discussed in this paper. Lurching waves and the related bifurcations might be experimentally observable by recording from populations of direction selective neurons. The neurons first would have to be clustered according to their speed selectivity and the centers of their receptive fields. The responses would have to be time aligned with respect to the stimulus. Then activity waves could potentially be observed either by simple histogramming within the different spatiotemporal bins, or by using more sophisticated techniques for interpolation, either based on standard regularization or Bayesian techniques [30–32]. A potential complication in the visual cortex might be that multiple populations of neurons with different speed selectivity might inhibit each other [8]. The same mechanism, however, might be relevant in other cortical areas as well, that are experimentally easier to access. One example is the direction-selective place cells in the hippocampus that have the advantage that multiunit recordings with more than 100 electrodes are possible [33].

ACKNOWLEDGMENTS

We acknowledge very helpful discussions with Dr. M. Goldman, Dr. D. Jin, Dr. T. Poggio, and Dr. H.S. Seung.

APPENDIX: STABILITY ANALYSIS

1. Stability of the traveling pulse solution in the step threshold model

The stability of the traveling pulse solution is analyzed by perturbing the stationary solution in the moving coordinate system. Let $\delta U(\xi,t)$ be a small perturbation of $U^*(\xi)$. The linearized perturbation dynamics reads

$$\tau\frac{\partial\delta U}{\partial t}-\tau v\frac{\partial\delta U}{\partial\xi}+\delta U(\xi,t) = -w(\xi-\xi_1^*)\delta\xi_1+w(\xi-\xi_2^*)\delta\xi_2, \quad \text{(A1)}$$

where $\delta\xi_i$ $(i=1,2)$ are the perturbations of the boundary points of the exited regime from the stationary values of ξ_i^* with $\xi_i=\xi_i^*+\delta\xi_i$ satisfying $U(\xi_i,t)=0$. Note that $\delta\xi_i$ is not independent of $\delta U(\xi,t)$, and the dependence can be found through

$$U(\xi_i^*+\delta\xi_i,t)=U(\xi_i^*,t)+\frac{\partial U(\xi_i^*,t)}{\partial\xi}\delta\xi_i+O(\delta\xi_i^2)=0.$$

Since $U(\xi_i^*,t)=\delta U(\xi_i^*,t)$, to the first order we have

$$\delta\xi_i=-\delta U(\xi_i^*,t)/c_i^*,$$

where $c_i^*\equiv dU^*(\xi_i)/d\xi$. Substituting this back into the perturbed dynamics, we derive the perturbed dynamics with perturbations in U only

$$\tau\frac{\partial\delta U}{\partial t}-\tau v\frac{\partial\delta U}{\partial\xi}+\delta U(\xi,t)=\frac{w(\xi-\xi_1^*)}{c_1^*}\delta U(\xi_1^*,t) -\frac{w(\xi-\xi_2^*)}{c_2^*}\delta U(\xi_2^*,t).$$

To check its stability, we substitute a solution of the form $\delta U(\xi,t)=e^{\lambda t}Y(\xi)$ into the above dynamics and derive the equation for $Y(\xi)$

$$-\tau vY'(\xi)+(1+\tau\lambda)Y(\xi)=\frac{w(\xi-\xi_1^*)}{c_1^*}Y(\xi_1^*) -\frac{w(\xi-\xi_2^*)}{c_2^*}Y(\xi_2^*).$$

We solve this equation by first assuming that $Y(\xi_1^*)$ and $Y(\xi_2^*)$ are constant, and afterwards we give self-consistent conditions for the solutions at ξ_1^* and ξ_2^* to satisfy. The solution of the above equation is

$$Y(\xi)=\frac{K(\xi-\xi_1^*)}{c_1^*(1+\tau\lambda)}Y(\xi_1^*)-\frac{K(\xi-\xi_2^*)}{c_2^*(1+\tau\lambda)}Y(\xi_2^*), \quad \text{(A2)}$$

The solution $Y(\xi)$ in Eq. (A2) has to satisfy two self-consistency equations for the solutions at ξ_1^* and ξ_2^*

$$Y(\xi_1^*)=\frac{K(0)}{c_1^*(1+\tau\lambda)}Y(\xi_1^*)-\frac{K(\xi_1^*-\xi_2^*)}{c_2^*(1+\tau\lambda)}Y(\xi_2^*),$$

$$Y(\xi_2^*)=\frac{K(\xi_2^*-\xi_1^*)}{c_1^*(1+\tau\lambda)}Y(\xi_1^*)-\frac{K(0)}{c_2^*(1+\tau\lambda)}Y(\xi_2^*).$$

For the above equations to have a solution, the transcendental Eq. (9) has to be satisfied. From this equation the eigenvalues λ can be found numerically. The traveling pulse solution is asymptotically stable only if the real parts of all eigenvalues λ that solve Eq. (9) are nonpositive.

2. Stability of the traveling pulse solution in the linear threshold model

The stability analysis is carried out by perturbing the dynamics of the Fourier components in Eqs. (25)–(27). The general procedure is to perturb the dynamics first, which involves the perturbation of terms such $\delta\theta_c$, $\delta\Phi$, and $\Delta I_1(t)$. To determine these terms, we subsequently perturb Eqs. (21)–(23). Defining $\tilde{\Phi}\equiv\Phi-\theta_0$ and $\tilde{\Psi}\equiv\Psi-\theta_0$, the perturbed linearized dynamics can be summarized as follows:

$$\tau\delta\dot{r}_0=\left(\frac{J_0\theta_c}{\pi}-1\right)\delta r_0+J_1\cos(\tilde{\Phi}-\tilde{\Psi}+\beta)\frac{\sin(\theta_c)}{\pi}\delta r_1 -\epsilon C\sin(\tilde{\Phi})\frac{\sin(\theta_c)}{\pi}\delta\tilde{\Psi},$$

$$\tau\delta\dot{r}_1=\cos(\tilde{\Phi}-\tilde{\Psi})\frac{\sin(\theta_c)}{\pi}J_0\delta r_0+\left(-1+J_1\left\{\frac{\theta_c}{2\pi}\cos(\beta) +\frac{\sin(2\theta_c)}{4\pi}\cos[2(\tilde{\Phi}-\tilde{\Psi})+\beta]\right\}\right)\delta r_1 -\epsilon C\left\{\frac{\theta_c}{2\pi}\sin(\tilde{\Psi})+\frac{\sin(2\theta_c)}{4\pi}\sin(2\tilde{\Phi}-\Psi)\right\}\delta\tilde{\Psi},$$

$$\tau r_1\delta\dot{\tilde{\Psi}}=\sin(\tilde{\Phi}-\tilde{\Psi})\frac{\sin(\theta_c)}{\pi}J_0\delta r_0+\left(-\tau v-J_1\left\{\frac{\theta_c}{2\pi}\sin(\beta) -\frac{\sin(2\theta_c)}{4\pi}\sin[2(\tilde{\Phi}-\tilde{\Psi})-\beta]\right\}\right)\delta r_1 -\epsilon C\left\{\frac{\theta_c}{2\pi}\cos(\tilde{\Psi})-\frac{\sin(2\theta_c)}{4\pi}\cos(2\tilde{\Phi}-\Psi)\right\}\delta\tilde{\Psi}.$$

To determine the stability of the traveling pulse solution, we have to analyze the dynamics of these three coupled differential equations. If $\epsilon C\ll 1$, then the dynamics of $\delta\dot{\tilde{\Psi}}$ is decoupled from that of δr_0 and δr_1 and the stability condition can be approximated by the stability of the two dynamics Eqs. (32) and (33).

[1] W. Reichardt, in *Sensory Communication*, edited by A. Rosenblith (MIT Press, Cambridge, MA, Wiley, New York, 1961), pp. 303–317.
[2] C. Koch and T. Poggio, in *Models of the Visual Cortex*, edited by D. Rose and V. G. Dobson (Wiley, New York, 1989), pp. 15–34.
[3] J. P. van Santen and G. Sperling, J. Opt. Soc. Am. A **256**, 300 (1985).
[4] E. H. Adelson and J. R. Bergen, J. Opt. Soc. Am. A **256**, 284 (1985).
[5] A. B. Watson and A. J. Ahumada, J. Opt. Soc. Am. A **256**, 322 (1985).
[6] H. Suarez, C. Koch, and R. Douglas, J. Neurosci. **15**, 6700 (1995).
[7] R. Maex and G. A. Orban, J. Neurophysiol. **75**, 1515 (1996).
[8] P. Mineiro and D. Zipser, Neural Comput. **10**, 353 (1998).
[9] D. Golomb, X. J. Wang, and J. Rinzel, J. Neurophysiol. **75**, 750 (1996).
[10] J. Rinzel, D. Terman, X. Wang, and B. Ermentrout, Science **279**, 1351 (1998).
[11] D. Golomb and G. B. Ermentrout, Proc. Natl. Acad. Sci. U.S.A. **96**, 13480 (1999).
[12] D. Golomb and G. B. Ermentrout, Phys. Rev. Lett. **86**, 4179 (2001).
[13] M. von Krosigk, T. Bal, and D. A. McCormick, Science **261**, 361 (1993).
[14] T. Bal, M. von Krosigk, and D. A. McCormick, J. Physiol. (London) **261**, 641 (1995).
[15] S. P. Sabatini and F. Solari, Biol. Cybern. **80**, 171 (1999).
[16] G. B. Ermentrout and J. B. McLeod, Proc. R. Soc. Edinburgh, Sect. A: Math. **123**, 461 (1993).
[17] S. Amari, Biol. Cybern. **27**, 77 (1977).
[18] D. Hansel and H. Sompolinsky, in *Methods in Neuronal Modeling*, edited by C. Koch and I. Segev (MIT Press, Cambridge, MA, 1998), pp. 499–567.
[19] D. J. Pinto and G. B. Ermentrout, SIAM (Soc. Ind. Appl. Math.) J. Appl. Math. **62**, 206 (2001).
[20] D. J. Pinto and G. B. Ermentrout, SIAM (Soc. Ind. Appl. Math.) J. Appl. Math. **62**, 226 (2001).
[21] H. R. Wilson and J. D. Cowan, Kybernetik **13**, 55 (1973).
[22] R. Ben-Yishai, R. L. Bar-Or, and H. Sompolinsky, Proc. Natl. Acad. Sci. U.S.A. **92**, 3844 (1995).
[23] E. Salinas and L. F. Abbott, Proc. Natl. Acad. Sci. U.S.A. **93**, 11956 (1996).
[24] M. A. Giese, *Dynamic Neural Field Theory of Motion Perception* (Kluwer Academic, Dordrecht, 1999).
[25] D. Golomb and G. B. Ermentrout, Network Comput. Neural Syst. **11**, 221 (2000).
[26] R. Hahnloser, R. J. Douglas, M. Mahowald, and K. Hepp, Nat. Neurosci. **2**, 746 (1999).
[27] M. Carandini and D. Ferster, J. Neurosci. **20**, 470 (2000).
[28] K. Zhang, J. Neurosci. **16** (6), 2112 (1996).
[29] D. Pelinovsky and V. Yakhno, Neural Networks **4**, 443 (1993).
[30] D. Jancke, W. Erlhagen, H. R. Dinse, A. C. Akhavan, M. Giese, A. Steinhage, and G. Schöner, J. Neurophysiol. **19**, 9016 (1998).
[31] P. A. Zemel and P. Dayan, Neural Comput. **10**, 403 (1998).
[32] K. Zhang, I. Ginzburg, B. L. McNaughton, and T. J. Sejnowski, J. Neurophysiol. **79**, 1017 (1998).
[33] M. R. Mehta, M. C. Quirk, and M. A. Wilson, Neuron **25**, 707 (2000).
[34] Our analysis can be generalized to the case with multiple excited regimes resulting in more complex equations. Only neurons inside the excited regime contribute to the integral.